

# A linear approximation to steady flows at moderate Reynolds numbers

By **MARCUS ROPER AND MICHAEL P. BRENNER**

School of Engineering and Applied Sciences, Harvard University, Cambridge, MA 02138, USA

(Received ?? and in revised form ??)

We present a simple generalization of Oseen’s equation that captures the drag-determining features of steady flow around bluff bodies up to Reynolds numbers in the tens or hundreds. The approximation is applied to two flow problems – finding the speed at which flow around a steadily translating sphere first separates, and determining the shape of the perfect projectile. We present a partial explanation for the success of the approximation, showing how varying the parameter that appears in the system of equations tunes the length scale on which it accurately renders kinematical features of the flow around a point-force singularity.

---

Modeling of flow around moving bodies at Reynolds numbers between 1 and 100 presents great analytical challenges. These challenges derive in part from the complexity of the velocity field, which, as the flow speed is increased, passes through an ordered sequence of topological transitions, starting with the appearance of a ring-eddy behind the body and culminating with the unsteady break-down and partial shedding of this eddy into a street of vortex loops (Batchelor 1967; Taneda 1956).

Analytical approaches have enjoyed much greater success in cases where inertial terms may be completely neglected (the Stokes flow limit), reducing the governing momentum balance to a set of linear equations that – at least for high symmetry bodies – may often be solved analytically.

A formally correct method for incorporating arbitrarily weak inertial stresses into these equations is already known. Oseen (1927) showed that Stokes’ equations could be modified to include leading order inertial effects while retaining the core properties of linearity and reciprocity that make them analytically tractable. Oseen’s approximation, in which the momentum balance is supplemented by a term representing the transport of momentum by the uniform stream, is certainly applicable far from the body where it reduces to linearisation of the full Navier-Stokes equations, but incorrectly renders flow features near the body, where the body-induced disturbance to the uniform flow is not small. Chester (1962) and Brenner & Cox (1963) showed that Oseen’s equations nevertheless correctly predict the leading-order contribution of fluid inertia to the drag experienced by the body.

Proudman & Pearson (1957) provided a framework for the systematic inclusion of weak inertial effects by introducing two perturbation expansions for separate regions of the flow: a region with typical dimension equal to the size of the body (which we denote by  $a$ ), in which the leading order dynamics are Stokesian, and a far field, in which flow variations occur on an  $O(a/Re)$  length scale and the dominant physical balance is given by Oseen’s approximation. The flows in the two regions are matched on some intermediate length-scale and the drag thereby expanded as a singular perturbation series in powers of  $Re$  and  $\log Re$ . The drag dependency upon Reynolds number thus computed has been

broadly confirmed by comparison with very precise measurements of the drag upon a sphere (Maxworthy 1965).

Although a fluid mechanician implementing the formalism of Proudman & Pearson (1957) is presented with a task no more analytically onerous than solving Oseen's equations with distributed forcing at each order of  $Re$ , the series that may thereby be obtained are not convergent – inclusion of more terms actually reduces the range of Reynolds numbers over which the series may be applied. In practise the formalism is useless for computation of drag at Reynolds numbers exceeding 1. Attempts to enlarge the domain of validity of the drag series have focused upon completing the series, either in an uncontrolled manner by using the renormalisation group to reorganise terms in the expansion (Veysey & Goldenfeld 2006) or by matching to a postulated high Reynolds number asymptote (see Proudman's Appendix to Chester & Breach 1969), but have not yielded any direct or generally applicable methods for computing analytically the drag upon a moving body at Reynolds numbers in the tens or hundreds.

In a previous article the authors found evidence that over this range of Reynolds numbers the underlying drag-determining features of the flow around a projectile retain the properties of linearity and reciprocity present in Stokes flows. We showed by direct computation that perfect projectiles – bodies of prescribed volume that are designed to suffer minimum fluid drag in steady flight – remain very fore-aft symmetric even at moderate Reynolds numbers, although the surrounding flow inevitably becomes highly asymmetric (Roper *et al.* 2007). It was demonstrated that this persistence of fore-aft symmetry could arise if the drag-determining features of the flow obeyed a form of the reciprocal theorem under reversal of the direction of flight of the body. Here we exploit this observation to construct a linear and reciprocal approximation to the flow that accurately reproduces the drag upon a steadily translating body up to moderate Reynolds numbers.

Save for their intrinsic elegance, analytical approximations for the moderate Reynolds number steady flow around a projectile may appear to have limited utility to the modern fluid mechanician. Although the problem of asymptotic modeling of fluid flows at or near the threshold for separation challenged our predecessors, it receives little attention now that advances in direct numerical simulation permit the unapproximated Navier-Stokes equations to be solved. Against such objections we present two applications of the modified Oseen approximations that have been selected in order to harness the linearity and reciprocity or the analytical tractability of the equations.

For the first application, we tackle the classical problem of understanding the first topological transition of the flow around a steadily translating sphere (Taneda 1956). The modified Oseen equations capture qualitative features of this transition, and can be solved analytically using convergent perturbation series.

For the second application we return to the practical problem introduced in Roper *et al.* (2007); design of perfect micro-projectiles. We draw inspiration here from the explosively launched meiospores of many species of fungi (Pringle *et al.* 2005; Vogel 2005). Although primarily wind-dispersed these propagules must pass through a thin boundary layer of still air that clings to the originating fruiting body. The parent fungus therefore benefits from enhanced fitness if its spores are shaped in order to minimize drag. Selection for drag-minimizing spore shapes is plausible only if a robust method for generating minimal drag shapes may be found. Here, we derive from the modified Oseen equations a gradient descent algorithm for making successive optimal corrections to the shape of a proto-projectile in order to evolve it to a minimum drag shape. Unlike previously implemented algorithms for computing minimal drag shapes (Pironneau 1974; Roper *et al.* 2007) the variational condition at the heart of this algorithm requires only evaluation of the shear

stress upon surface of the proto-projectile, needing no knowledge of the global flow field. With the ontogeny of fungal spores in mind, we also show how stresses may be used to template the growth or self-assembly of the perfect projectile, even if it is not exposed to flow, since the linearity of the approximating equations allows the surface shear stresses to be perfectly reproduced within an elastic medium with elastic strains standing in for fluid strain rates.

The accuracy of the modified Oseen equations in reproducing the drag upon micro-projectiles remains an empirical observation. In §5 we go some way toward its demystification through study of *single-scale* bodies: regions of fluid entrained within closed streamlines that are formed by the deceleration of fluid in a uniform stream under an applied point force, thereby creating bodies with slip surface boundary conditions. Tuning of the parameter in the modified Oseen equations, provides direct matching of the flow field upon the boundary of such a body, at the cost of losing fidelity in the the far field.

### 1. Structure of the moderate $Re$ equations.

Oseen’s equations do not accurately capture the contribution of finite fluid inertia to the force experienced by the body beyond a single correction at  $O(Re)$  to the Stokes drag and, like the formalism of Proudman & Pearson (1957), can not be used to compute the fluid drag when the Reynolds number of the body exceeds 1. Nonetheless they provide a route for adding inertial terms to Stokes’ equations without sacrificing reciprocity. Specifically, while the functional form of Oseen’s equations is retained, we allow the Reynolds number that appears therein to depart in a geometry-independent but nonlinear manner from the Reynolds number used in the Navier-Stokes equations. This extends a proposal made by Carrier (1953) for modifying Oseen’s equations in order to reproduce flow features close to the boundary of a steadily moving body. By empirically taking the Oseen Reynolds number to be a fixed multiple of the Reynolds number appearing in the Navier Stokes equations, Carrier was able to achieve empirically good agreement in drag for spheres, cylinders and flat plates at incidence over the range  $5 < Re < 25$ .

We derive our modification to Oseen’s equations by direct numerical matching of the drags upon a large number of steadily moving bluff bodies. The weight of our contention that the modified Oseen’s equations thus obtained have general applicability is carried by a numerical demonstration that the correspondence between the two Reynolds numbers is one-to-one and independent of the shape of the body.

### 2. Generalising Oseen’s approximation.

Oseen’s equations incorporate inertial effects by adding to Stokes’ equations a linearised version of the fully non-linear term that represents momentum advection in the Navier-Stokes equations, effectively treating the disturbance due to the body as a small correction to the far-field flow (Oseen 1927; Batchelor 1967). Taking a body-fixed coordinate system, with the body at rest and flow approaching from the negative  $z$ -direction, the flow field around the body is therefore governed by equations

$$Re_O \frac{\partial \mathbf{u}}{\partial z} = -\nabla p + \nabla^2 \mathbf{u} \quad \text{and} \quad \nabla \cdot \mathbf{u} = 0, \quad (2.1)$$

with the usual complement of boundary conditions. We have non-dimensionalised all lengths using  $a$ , the radius of a sphere of equivalent volume to the projectile, all speeds by  $U$ , the speed of flight of the projectile, and all stresses by  $\eta U/a$ . The relative strength of inertial to viscous stresses is encoded into a Reynolds number  $Re_O \equiv \rho U a / \eta$ . In order for

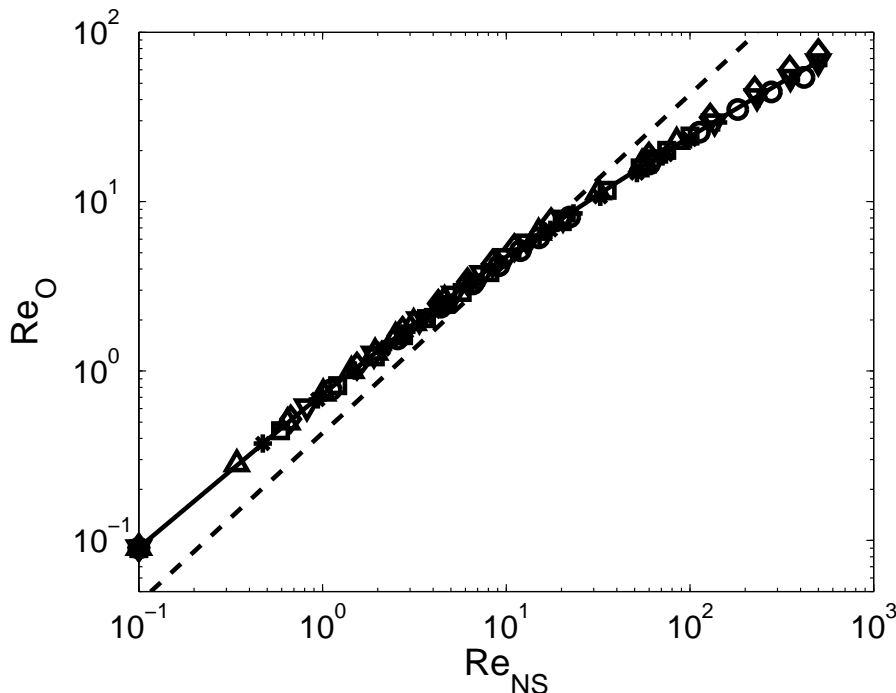


FIGURE 1. One-to-one identification of Oseen and Navier-Stokes Reynolds numbers for spheroids of aspect ratios  $2/3$  ( $\square$ ),  $1$  ( $\circ$ ),  $4/3$  ( $*$ ),  $2$  ( $+$ ),  $3$  ( $\nabla$ ),  $4$  ( $\triangle$ ),  $5$  ( $\diamond$ ). The solid curve is a best fit, and the dashed curve is the hypothesis of Carrier ( $\mathcal{R}e_O = 0.43\mathcal{R}e_{NS}$ )

the far-field limit of the Navier-Stokes and Oseen's equations to agree it is conventional to identify the two dimensionless groups, but we distinguish between them using subscripts:  $\mathcal{R}e_O$  for Oseen's equations and  $\mathcal{R}e_{NS}$  for the Reynolds number appearing in the Navier-Stokes equations. Proudman & Pearson (1957) and Brenner & Cox (1963) showed that if the two Reynolds numbers are made equal then the Oseen equations correctly predict the drag force upon the body up to  $O(\mathcal{R}e)$  corrections in the limit as  $\mathcal{R}e \rightarrow 0$ .

We relax the requirement that the approximate velocity field agree with the Navier-Stokes flow in the far field, and instead focus upon reproducing the drag-determining features of the near-field flow, looking for a geometry-independent method for selecting  $\mathcal{R}e_O$ , given  $\mathcal{R}e_{NS}$ , in order to predict the drag upon the projectile. Carrier (1953) argued for  $\mathcal{R}e_O = 0.43\mathcal{R}e_{NS}$  using limited experimental data supplemented by asymptotic study of the boundary layer structure near the leading edge of a flat plate at incidence to flow. Numerical computation of the flow around a body using the commercial finite element software COMSOL Multiphysics allows the relationship between  $\mathcal{R}e_O$  and  $\mathcal{R}e_{NS}$  to be computed directly. For any Navier-Stokes Reynolds number we may solve for the flow field around the projectile and thence compute the drag. We repeat the computation using Oseen's equations, tuning  $\mathcal{R}e_O$  so that the Oseen drag equals the Navier-Stokes drag upon the body. The viability of the modified-Oseen equations is pinned to the universality of the dependence of  $\mathcal{R}e_O$  upon  $\mathcal{R}e_{NS}$  among bodies of different shapes. As Figure 1 shows, repeating the matching process for spheroids of different aspect ratios gives us, in all cases, the same value of  $\mathcal{R}e_O$  for each value of  $\mathcal{R}e_{NS}$ .

Regarding the geometrical invariance of the correspondence between Navier-Stokes

and Oseen’s Reynolds numbers as a serendipitous but nonetheless established result, we proceed directly to consider two applications.

### 3. Application I: Topological transitions in flow around a sphere.

We test whether the modified Oseen’s equations are able to reproduce features of the flow field near the projectile, in addition to the fluid drag. Of particular interest is the emergence, for sufficiently high speed projectiles, of a ring eddy that travels steadily behind the bluff body. *A posteriori* support for supposing that the same transition will be seen in the modified Oseen representation of the flow is provided by Section 5, in which it is shown that the modified Oseen equations can be applied to a more general set of boundary conditions than no-slip. Regarding the separation bubble that demarcates between the ring eddy and open streamlines in the rest of the flow as such a generalised boundary, we posit that the accuracy of the modified-Oseen representation of the total fluid drag upon the generalised body surface requires that the approximation also correctly renders some geometrical features of this separation bubble.

The development from creeping flow into the separation bubble is shown in Figure 2(a-d), in which the exact streamlines (left panels) are compared with the predictions of the modified Oseen approximation (right panels). The adequacy of the approximate equations in reproducing the width and length of the separation bubble near the critical Reynolds number at which the eddy first appears may be judged more precisely from panels (e-f) of the figure. The modified Oseen equations slightly under-predict the critical Reynolds number at which separation first occurs, giving a critical Reynolds number of  $\mathcal{Re}_O = 3.7$  which maps to  $\mathcal{Re}_{NS} = 7.3$  under the correspondence shown in Figure 1, while the un-approximated equations give  $\mathcal{Re}_{NS} = 10$ . The modified Oseen equations correctly predict a bubble that increases in width like  $\sim (\mathcal{Re} - \mathcal{Re}_c)^{1/2}$  and in length like  $\sim (\mathcal{Re} - \mathcal{Re}_c)$  but slightly under predict the prefactors in both of these relations, thereby tending to produce shorter and more slender ring eddies than are actually observed. The maximum discrepancy between the dimensions of approximate and exact ring eddies remains less than 18% in length and 15% in width, below  $\mathcal{Re}_{NS} = 100$ . Beyond this order of Reynolds number experimental observations show that the ring eddies start to vibrate irregularly, so that simulations of steady flow may no longer be appealed to (Taneda 1956).

As we have already noted, analytical prediction from the unapproximated equations of the exact onset of separation and subsequent growth of the ring eddy is highly challenging. By contrast, for simple flow geometries such as flow around a sphere, the corresponding modified-Oseen’s equations may be solved analytically by regular series expansions.

It is known that perturbation expansions for the Oseen velocity field as powers of  $\mathcal{Re}_O$  tend to have finite radii of convergence and can not in most circumstances be directly evaluated at Reynolds numbers large to trigger flow separation. For spherical projectiles, Goldstein (1929*b*) estimated that the series expansion for the flow field diverged at  $\mathcal{Re}_O \approx 1$ . van Dyke (1970) showed using the method of Domb & Sykes (1957) that divergence is provoked by an isolated simple pole at  $\mathcal{Re}_O = -\mathcal{Re}_c = 2.09091$ . Thus, in order to develop analytic expressions for the separated flow field we make an Euler transformation  $\epsilon = \mathcal{Re}/(\mathcal{Re} + \mathcal{Re}_c)$  that eliminates this simple pole, and expand using  $\epsilon$  as the small parameter. Introduce a system of spherical polar coordinates  $(r, \theta, \phi)$  with the polar direction  $\theta = 0$  pointing along the  $z$ -axis. We can define a streamfunction,  $\psi$ , for the velocity field so that:

$$u_r = \frac{1}{r^2 \sin \theta} \frac{\partial \psi}{\partial \theta}, \quad u_\theta = -\frac{1}{r \sin \theta} \frac{\partial \psi}{\partial r}, \quad (3.1)$$

thereby automatically satisfying the incompressibility constraint. The vorticity equation (formed by taking the curl of Oseen's equation (2.1)) may then be written as:

$$\mathcal{E}_r^4 \psi = \mathcal{R}e_c \epsilon (1 + \epsilon + \epsilon^2 + \dots)(1 - \beta^2) \mathcal{L}_r \mathcal{E}_r^2 \psi, \quad (3.2)$$

in which we have defined operators

$$\mathcal{E}_r^2 \equiv \frac{\partial^2}{\partial r^2} + \frac{1 - \beta^2}{r^2} \frac{\partial^2}{\partial \beta^2} \quad \text{and} \quad \mathcal{L}_r \equiv \frac{\beta}{1 - \beta^2} \frac{\partial}{\partial r} + \frac{1}{r} \frac{\partial}{\partial \beta}, \quad (3.3)$$

and a transformed meridional ordinate  $\beta = \cos \theta$ . We solve this equation by developing simultaneous expansions for the streamfunction in the *Stokes* and *Oseen* layers, with respective distance variables  $r$  and  $\lambda = \mathcal{R}e_c \epsilon r$  (Proudman & Pearson 1957). Within the Oseen layer we define a rescaled streamfunction  $\psi(r, \beta) = \Psi(\lambda, \beta) / \epsilon^2 \mathcal{R}e_c^2$ , and operators  $\mathcal{E}_r^2 = \mathcal{R}e_c^2 \epsilon^2 \mathcal{E}_\lambda^2$ , and  $\mathcal{L}_r = \mathcal{R}e_c \epsilon \mathcal{L}_\lambda$ . The vorticity equation may then be recast as for the Oseen layer as

$$\mathcal{E}_\lambda^4 \Psi - (1 - \beta^2) \mathcal{L}_\lambda \mathcal{E}_\lambda^2 \Psi = \epsilon (1 + \epsilon + \epsilon^2 + \dots)(1 - \beta^2) \mathcal{L}_\lambda \mathcal{E}_\lambda^2 \psi. \quad (3.4)$$

Expand the Stokes layer streamfunction in powers of  $\epsilon$ :  $\psi \equiv \sum_{n=0}^{\infty} \epsilon^n \psi_n$  (and similarly within the Oseen layer). The summands in this expansion can be found using the procedure for matching the expansions of Proudman & Pearson (1957). The first term in the Stokes layer expansion and the first and second terms of the Oseen layer expansion agree with the terms exhibited by Proudman & Pearson (1957) in their analysis of the full Navier-Stokes equations:

$$\psi_0 = - \left( r^2 - \frac{3r}{2} + \frac{1}{2r} \right) Q_1 \quad (3.5)$$

$$\Psi_0 = \frac{1}{2} \lambda^2 (1 - \beta^2) \quad (3.6)$$

$$\Psi_1 = -\frac{3}{2} Q_0 \left( 1 - e^{-\lambda(1-\beta)/2} \right), \quad (3.7)$$

where dependence of the Stokes layer streamfunction upon meridional position is expressed by expansion into Gegenbauer polynomials  $Q_n(\beta) = \int_{-1}^{\beta} P_n(\beta') d\beta'$ , where  $P_n(\beta)$  are Legendre polynomials.

At  $O(\epsilon)$  in the Stokes layer, we must solve

$$\mathcal{E}_r^4 \psi_1 = \mathcal{R}e_c (1 - \beta^2) \mathcal{L}_r \mathcal{E}_r^2 \psi_0, \quad (3.8)$$

subject to vanishing velocity on the boundary of the sphere and to the matching constraint

$$\lim_{\lambda \rightarrow 0} \Psi = \mathcal{R}e_c^2 \epsilon^2 \lim_{r \rightarrow \infty} \psi, \quad (3.9)$$

which yields, at this order:  $\psi_1 \sim -\frac{3\mathcal{R}e_c}{8} r^2 (Q_1 - Q_2)$  as  $r \rightarrow \infty$ . The solution is

$$\psi_1 = -\frac{3\mathcal{R}e_c}{8} \left( r^2 - \frac{3r}{2} + \frac{1}{2r} \right) Q_0 + \frac{3\mathcal{R}e_c}{8} \left( r^2 - 2 + \frac{1}{r^2} \right) Q_2. \quad (3.10)$$

At next order in the Oseen region, we obtain

$$\mathcal{E}_\lambda^4 \Psi_2 - (1 - \beta^2) \mathcal{L}_\lambda \mathcal{E}_\lambda^2 \Psi_2 = (1 - \beta^2) \mathcal{L}_\lambda \mathcal{E}_\lambda^2 \Psi_1, \quad (3.11)$$

while an appeal to the matching condition (3.9) produces  $\Psi \sim \frac{9\mathcal{R}e_c^2}{16} \lambda Q_1$  as  $\lambda \rightarrow 0$ .

Goldstein's transformation  $\mathcal{E}_\lambda^2 \Psi_2 = \Phi_2 e^{\lambda\beta/2}$  then yields

$$\left(\mathcal{E}_\lambda^2 - \frac{1}{4}\right) \Phi_2 = -\frac{3\mathcal{R}e_c}{4} \left(1 + \frac{2}{\lambda}\right) e^{-\lambda/2} Q_1 + \frac{3\mathcal{R}e_c}{4} \left(1 + \frac{6}{\lambda} + \frac{12}{\lambda^2}\right) e^{-\lambda/2} Q_2, \quad (3.12)$$

or

$$\mathcal{E}_\lambda^2 \Psi_2 = \mathcal{R}e_c \left[ \left( \frac{3\lambda}{4} + A_1 \sqrt{\frac{\lambda}{\pi}} K_{3/2}(\lambda/2) \right) Q_1 - \frac{3\lambda}{4} \left(1 + \frac{2}{\lambda}\right) Q_2 \right] e^{-\lambda(1-\beta)/2} \quad (3.13)$$

where the value of the constant  $A_1$  (representing a solution of the homogenous system  $(\mathcal{E}_\lambda^2 - \frac{1}{4}) \Phi_2 = 0$  can be determined from the matching constraint  $\mathcal{E}_\lambda^2 \psi \sim -\frac{9\mathcal{R}e_c^2}{8\lambda} Q_1$  so that  $A_1 = -\frac{9}{16} \mathcal{R}e_c^2$ . One more inversion gives

$$\Psi_2 = \frac{3\mathcal{R}e_c}{2} \left(1 - \frac{3\mathcal{R}e_c}{8}\right) Q_0 \left(1 - e^{-\lambda(1-\beta)/2}\right) + \frac{3\mathcal{R}e_c \lambda}{2} Q_1 e^{-\lambda(1-\beta)/2}. \quad (3.14)$$

Integration of the corresponding equations for the Stokes layer gives the  $O(\epsilon^2)$  contribution to the streamfunction

$$\begin{aligned} \psi_2 = & \frac{3\mathcal{R}e_c}{8} \left( \frac{\mathcal{R}e_c r^3}{5} - \left(1 + \frac{3\mathcal{R}e_c}{8}\right) r^2 + \frac{3r}{2} \left(1 + \frac{13\mathcal{R}e_c}{120}\right) - \frac{1}{2r} \left(1 - \frac{\mathcal{R}e_c}{40}\right) \right) Q_1 \\ & + \frac{\mathcal{R}e_c}{8} \left( -\mathcal{R}e_c r^3 + 3r^2 \left(1 + \frac{3\mathcal{R}e_c}{8}\right) - 6 \left(1 - \frac{\mathcal{R}e_c}{24}\right) + \frac{3}{r^2} \left(1 - \frac{\mathcal{R}e_c}{8}\right) \right) Q_2 \\ & + \frac{\mathcal{R}e_c^2}{20} \left( r^3 - 3r + \frac{3}{r} - \frac{1}{r^3} \right) Q_3. \end{aligned} \quad (3.15)$$

Greater accuracy may be achieved by the tedious but straightforward process of including terms of higher order in  $\epsilon$  (see panel (e) of Figure 2), since the series is absolutely convergent if  $|\epsilon| < 1$ , or equivalently;  $\Re\{\mathcal{R}e\} > -\frac{1}{2}\mathcal{R}e_c$ . Nonetheless, as Figure 2(e-f) shows, a three-term truncation of the series  $\psi = \psi_0 + \epsilon\psi_1 + \epsilon^2\psi_2$  is sufficient to well approximate the critical value of  $\mathcal{R}e_O$  at which separation first occurs, as well as the initial growth of the separation bubble.

#### 4. Application II. Design of drag-minimising shapes

The linearity and reciprocity under flow reversal of the modified Oseen's equations may be exploited in the practical problem of self-assembling or growing perfect projectiles – bodies of prescribed volume that are engineered to experience the minimum possible drag in flight.

The perfect projectile criterion was derived by the authors in a previous article (Roper *et al.* 2007), as a variant of a criterion previously derived by Pironneau (1974). It was shown that for the drag upon the projectile to be unimprovable by any small, volume preserving, perturbation of its shape, the quantity  $J \equiv \frac{\partial \mathbf{u}}{\partial n} \cdot \frac{\partial \mathbf{w}}{\partial n}$  must be uniform over the entire of the boundary of the projectile. Here we write  $\partial/\partial n$  for the derivative in the body-normal direction. The *adjoint field*  $\mathbf{w}$  arises as a Lagrange multiplier enforcing conservation of momentum in the variational formulation of the Navier-Stokes equations. In practise  $\mathbf{w}$  must be solved for separately from  $\mathbf{u}$  by integration of a second order linear partial differential equation whose coefficients depend upon the components of the physical velocity field. Determining  $J$  for a given projectile shape therefore requires knowledge of the velocity field throughout the entire of the fluid-filled domain.

Our route to the growth of a drag-minimising projectile is to start with an arbitrarily shaped proto-projectile and to use the computed  $J$ -distribution to construct successive

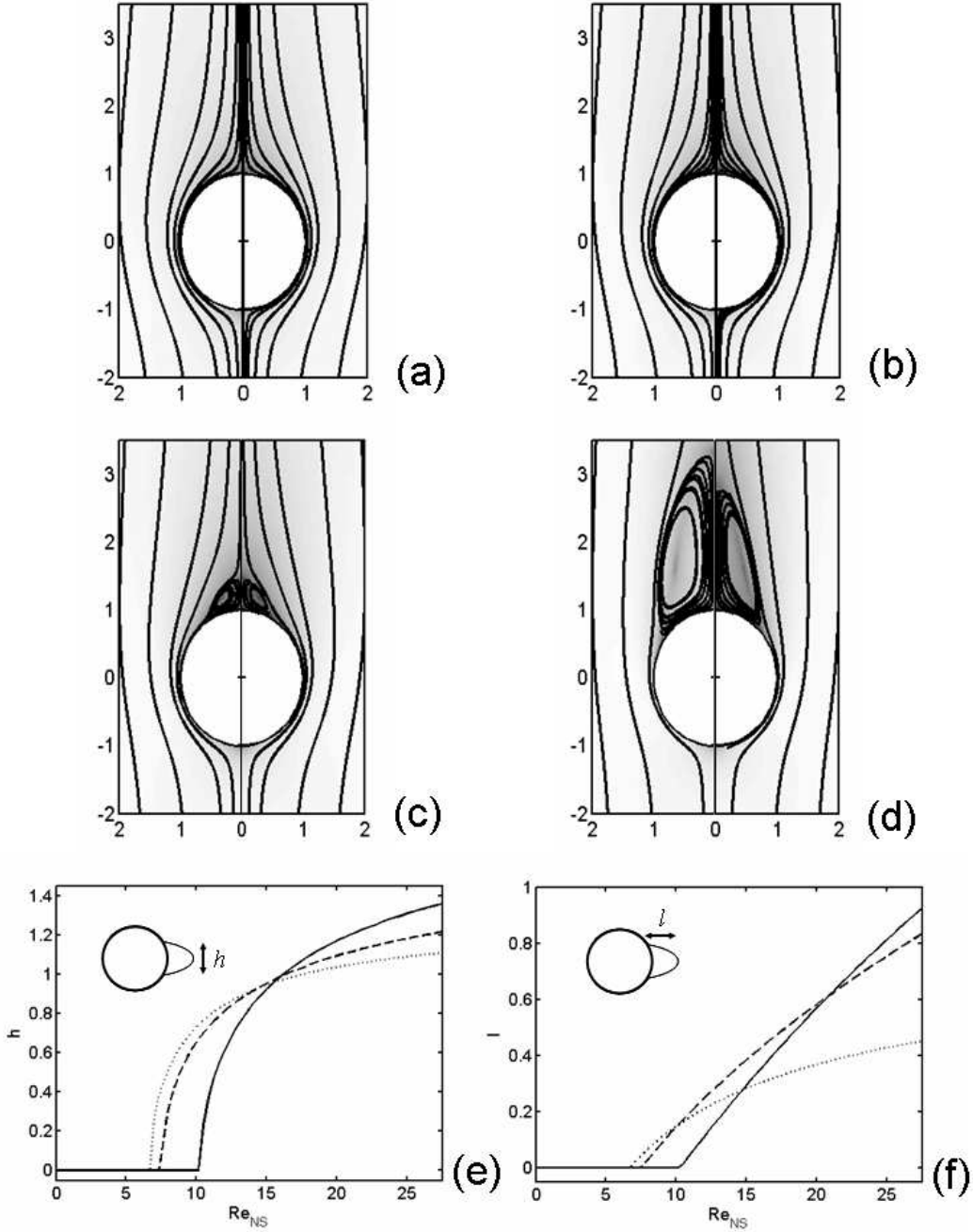


FIGURE 2. Comparison of Navier-Stokes (left panel) and modified-Oseen (right panel) representations of the flow field around a steadily translating sphere at (a)  $\mathcal{R}e_{NS} = 5.0$ ,  $\mathcal{R}e_O = 2.63$ , (b)  $\mathcal{R}e_{NS} = 9.0$ ,  $\mathcal{R}e_O = 4.14$  (c)  $\mathcal{R}e_{NS} = 18.0$ ,  $\mathcal{R}e_O = 6.96$  (d)  $\mathcal{R}e_{NS} = 72$ ,  $\mathcal{R}e_O = 18.92$ . The flow field is visualised by stream-lines (contours) and flow speed (shading). Geometry of the separation bubble: (f) width  $h$  and (g) length  $l$  of the separation bubble. The solid curves give the Navier-Stokes representation of the separation bubble and the dashed curves the solution of the modified Oseen equations. Dotted curves show the values given by a three term perturbation series solution of the modified-Oseen equations (3.15).

small perturbations to the boundary of the projectile (Roper *et al.* 2007). Such a shape-selection algorithm could only be implemented in a physical self-assembly or growth process if it were possible to relate the drag variation  $J$  in a simple manner to measurable properties of the flow such as the boundary stress.

The modified Oseen approximation for the fluid drag upon a steadily-moving body permits drastic simplification of the perfect projectile criterion. For flows governed by the modified Oseen's equations it can be shown (see Section 5) that the variation of drag upon the projectile due to a small perturbation of the body boundary also requires making the product of shear and adjoint shear uniform over the projectile boundary, but that the equation governing the adjoint field  $\mathbf{w}$  simplifies to:

$$-\mathcal{R}e_O \frac{\partial \mathbf{w}}{\partial z} = -\nabla q + \nabla^2 \mathbf{w} \quad (4.1)$$

in addition to an incompressibility constraint  $\nabla \cdot \mathbf{w} = 0$ , and with boundary conditions  $\mathbf{w} = \mathbf{0}$  on the surface of the body and  $\mathbf{w} \rightarrow -\mathbf{e}_z$  in the far-field.  $\mathbf{w}$  is thus the *reversed flow* that the projectile would encounter if it were to travel tail-first rather than nose-first through the fluid. For a fore-aft symmetric test projectile, the drag-variational  $J$  is then equal to the fore-aft symmetrised fluid shear stress upon the surface of the body.

Figure 3 evaluates the ‘almost-perfect’ projectiles produced according to this criterion. At each iteration of the ‘almost-perfect’ projectile generating algorithm, the Navier-Stokes equations are solved for the flow around a steadily translating fore-aft symmetric test projectile, the symmetrised-shear stress is computed, and the optimum fore-aft symmetric shape perturbation found. Just as in our previous study, numerical stability of the algorithm is enhanced if the locus of shapes between the initial test projectile and the almost perfect projectile is taken to be continuously parametrised by a deformation parameter, and an adaptive step-size integration routine used to advance the deformation parameter between intermediate shapes.

The drag upon a steadily translating almost perfect projectile approaches very closely to the minimum realisable drag over the range of Reynolds number assayed here ( $0.1 < \mathcal{R}e_{NS} < 100$ ), and imperfect projectiles resemble perfect projectiles even in respect of features, such as the cones on the front and rear, that can be shown to contribute only weakly to the total drag upon the body.

Cell growth is known to be sensitively actuated by fluid stresses (Davies 1989; LaBarbera 1990; Shraiman 2005), so growth toward a condition of uniform symmetrised shear stress is a plausible scenario for the morphogenesis of an organism that is exposed to flow. We hypothesize that it also holds for the the formation of delimiting membranes during the ontogeny of explosively launched meiospores of ascomycete fungi (Read & Beckett 1996), although these develop within enclosed fruiting structures and are not exposed to moving fluid until the instant of ejection (Ingold 1971). However, the linearity of the modified Oseen approximation means that the fluid stress field can be precisely mimicked within an incompressible and isotropic but spatially heterogeneous elastic medium such as exists within a developing fungal ascus. Specifically if the ascospore initial is taken to be a rigid inclusion, and the surrounding cell matrix is an elastic medium with shear modulus  $\mu = \mu_0 \exp(-2\mathcal{R}e_O z)$ , then any small displacement of the projectile will engender elastic deformation that exactly duplicate the flow field that it would encounter in flight.

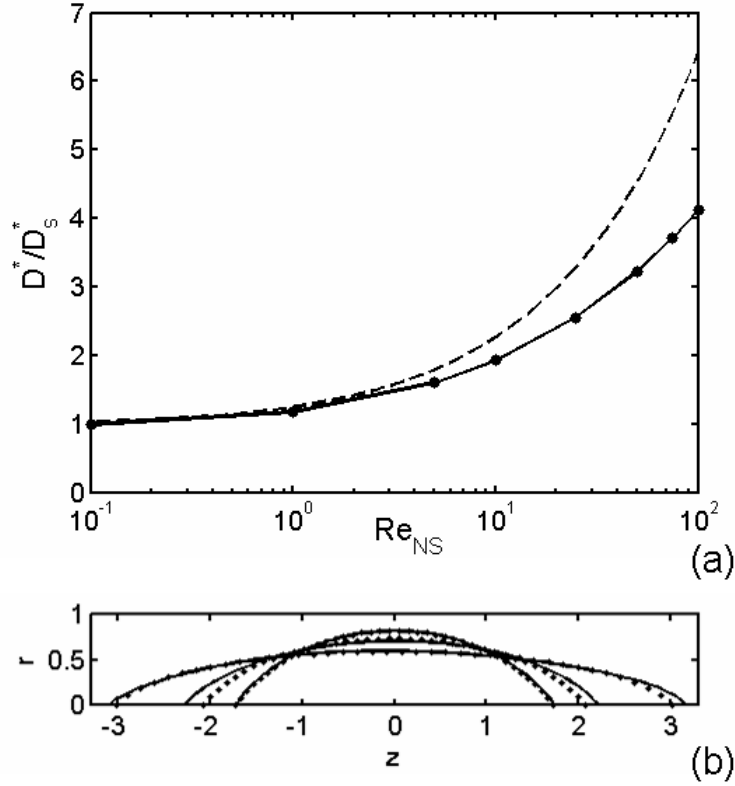


FIGURE 3. Comparison of approximate criteria for drag minimisation (a) Variation of drag (scaled by the  $Re = 0$  drag upon a sphere:  $D_s^* = 6\pi a\eta U$ ) with Reynolds number. The solid curve gives the minimum possible drag (on bodies satisfying the exact perfect projectile criterion) while the discrete data points correspond to almost perfect projectiles generated using the symmetrised shear stress criterion. The maximum discrepancy in drag between perfect and almost perfect projectiles is 0.08% over the range of Reynolds numbers shown here. For comparison we include the drag upon a sphere (dashed curve). (b) Comparison of perfect (solid curves) and almost perfect projectiles (dashed curves) for (in order of increasing aspect ratio)  $Re = 0.1, 10, 100$ .

## 5. Dissecting the modified-Oseen approximation.

In order to understand how the modified-Oseen's equations represent the flow of fluid around a steadily translating body, we consider the fluid drag upon a class of bodies that have much simpler velocity fields than the rigid-walled ellipsoidal projectiles hitherto studied. That is, consider the flow set up by a steadily translating point force  $F$  that moves in a direction parallel to the line of application of the force. When viewed in a frame of reference co-moving with the point force, the flow comprises two regions: a set of open streamlines representing fluid particles that are perturbed by the passage of the point force but that return to rest after it passes, and a region of closed streamlines, containing fluid that has been entrained by the moving point force (Figure 4).

We identify the separatrix between the regions of entrained and non-entrained fluid as an effective projectile boundary. The entire of the flow due to the translating point force may be reproduced by specification of a suitable slip velocity along the boundary. The available material constants allow a length scale to be defined for the problem: from the density  $\rho$ , viscosity  $\eta$  of the fluid and the strength  $F$  and speed of translation  $U$

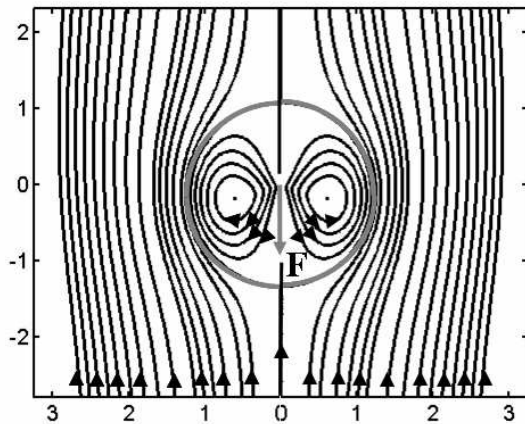


FIGURE 4. Streamlines associated with flow around a translating point force,  $\mathcal{Re} = 1.54$ , in the rest frame of the point force. The grey curve denotes the boundary of the associated *single-scale projectile*: the region of fluid entrained by the point force.

of the point force, we may define a length-scale  $a = F/6\pi\eta U$  and a Reynolds number  $\mathcal{Re} = \rho F/6\pi\eta^2$ . We have chosen our prefactors so that in the limit as  $\mathcal{Re} \rightarrow 0$ ,  $a$  is equal to the radius of the spherical rigid-walled projectile that traveling at the same speed,  $U$  would encounter the same fluid drag force  $F$ . The separatrix gives a projectile that is geometrically simpler than any previously considered, since it possesses only the single length scale,  $a$ , up to multiplication by arbitrary powers of  $\mathcal{Re}$ . Imposing other slip velocity distribution upon the separatrix would introduce higher order moments in the singularity system within the projectile and thereby add one or more additional length-scales.

Oseen's original approximation, formulated as a linearisation of the Navier-Stokes momentum balance equations designedly provide an asymptotically correct picture of the flow field far from the point force (with the length scale for the domain of applicability scaling as  $\sim a/\mathcal{Re}$  at small Reynolds numbers). Both Navier-Stokes and Oseen representations produce far field disturbances with mass inflow confined to a narrow paraboloidal wake region  $\mathcal{Re}r \lesssim 1/(1 - \cos\theta)$  and uniform radial mass efflux outside of the wake. It's accurate rendering of the leading order effect of weak inertia upon this far field flow is the root of how Oseen's original approximation provides accurate drag estimates at very small  $\mathcal{Re}$  (Brenner & Cox 1963; Cox 1965). By contrast, our modified version of Oseen's approximation must disagree with both Oseen's approximation, and with the Navier-Stokes representation of the flow in the far field. Since the modified-Oseen Reynolds number is in all cases less than the Navier-Stokes Reynolds number (see Figure 1) the modified Oseen-equations produce systematically broader wakes than the Navier-Stokes representation of the flow (Figure 5(b)). Nonetheless, the total flow of momentum in the wake is conserved between the two representations, being equal to the applied force in both cases (Goldstein 1929*a*, 1931).

In both their original and modified forms, Oseen's equations produce a defective picture of the flow near the point of application of the force, although in all cases flows become singular, with fluid velocities diverging like  $1/r$ . In the Navier-Stokes representation the flow velocity approaches asymptotically the Landau-Squires solution for a submerged jet (Landau & Lifschitz 1987, pages 81–83):  $\psi \sim \frac{2r}{\mathcal{Re}_{NS}} \frac{\beta^2 - 1}{1 + \beta_0 + \beta}$ , where we have nondimen-

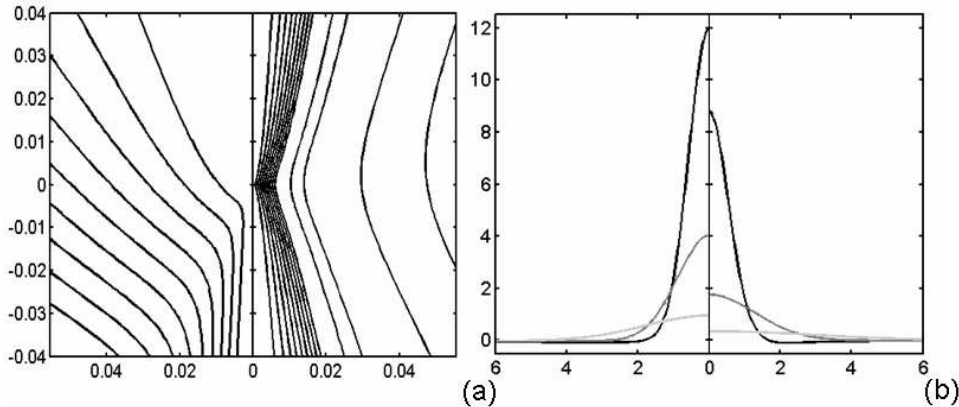


FIGURE 5. Navier-Stokes (left panel) and modified-Oseen (right panel) representations of the flow induced by a moving point force ( $\mathcal{R}e_{NS} = 34.8$ ,  $\mathcal{R}e_O = 11.8$ ). (a) The streamlines in the vicinity of the point force (located at the origin) and (b) the momentum flux in the wake defect  $\mathcal{R}e(1 - u_z)$  evaluated on surfaces  $z = 2$  (darkest), 10, 50 (lightest) (Goldstein 1929a).

sionalised  $\psi$  by  $Ua^2$  and the constant  $\beta_0$  may be related implicitly to the strength of the applied force by direct computation of the fluid stress upon an infinitesimal spherical surface centered upon the origin

$$\mathcal{R}e_{NS} = \frac{32}{9} \frac{1 + \beta_0}{\beta_0(2 + \beta_0)} + \frac{4}{3}(1 + \beta_0)^2 \log\left(\frac{\beta_0}{2 + \beta_0}\right) + \frac{8}{3}(1 + \beta_0). \quad (5.1)$$

As the Reynolds number is increased, the pattern of streamlines becomes markedly fore-aft asymmetric, with outflow focused into a conical jet of semi-angle  $\theta_0 \approx \sqrt{\frac{16}{9\mathcal{R}e_{NS}}}$  along the negative  $z$ -axis and mass inflow along parabolic streamlines outside of the jet. Contrast this with how the (modified-) Oseen's equations represent the flow field around a translating point force. The streamfunction is known exactly at all distances from the point of application of the force. It is simply the (modified-) Oseenlet field:

$$\psi_O = \frac{1}{2}(1 - \beta^2)r^2 - \frac{3}{2\mathcal{R}e_O}(1 + \beta)\left(1 - e^{-\mathcal{R}e_O r(1 - \beta)}\right), \quad (5.2)$$

so that as  $r \rightarrow 0$ ,  $\psi_O \sim \frac{3r}{4}(1 - \beta^2)$ . Near the point of application of the force, the modified-Oseen representation of the velocity field therefore differs from the exact flow field by showing neither localisation of mass efflux nor fore-aft symmetry breaking even at large Reynolds numbers. Two typical singular flow fields are set side by side in Figure 5(a). The contrast between the two representations is seen most sharply if the stress fields associated with the two singular flows are compared on an infinitesimal spherical surface. In the Navier-Stokes representation of the flow, the total force upon such a surface remains bounded (almost all of the work being done by the point force in accelerating fluid across the surface), and actually becomes negative at high Reynolds numbers, as the fluid hammer pressure supplies a reaction force upon the surface that points in the same direction to, rather than opposing to, the point force applied at the origin. In the modified Oseen equation, momentum flux across the control surface is always negligible, and the total fluid force upon the surface always equal and opposite to the applied force.

We postulate that the modified-Oseen equations produce an accurate picture of the fluid velocity field on some length scale intermediate between the two limits discussed above: accurately capturing the flow kinematics on slip-boundary of the single scale

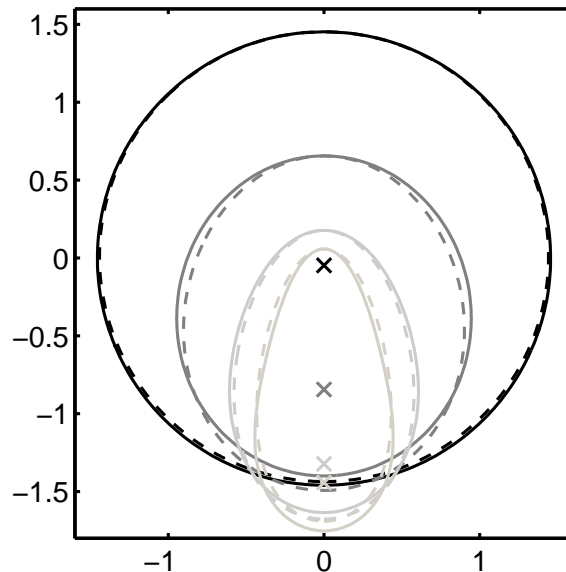


FIGURE 6. Comparison of single-scale bodies in the Navier-Stokes (solid curves) and modified-Oseen (dashed curves) representations. The projectiles are shaded according to Reynolds number:  $(\mathcal{Re}_O, \mathcal{Re}_{NS}) = (0.11, 0.13)$  (darkest),  $(3.09, 5.76)$ ,  $(11.75, 34.81)$  and  $(24.36, 101.30)$  (lightest). Crosses denote the location of the point force in the modified-Oseen representation. The point force is always located at the origin in the Navier-Stokes representation of the flow.

projectile, at the cost of producing defective kinematics both near the singularity and in the far field. Expecting to see close accord only in some local region, such as near the front stagnation point, which sets the thickness of the viscous boundary layer around the body, or on some gross measure such as the volume or surface area of the single-scale projectile, the authors were astonished to find that the separatrix shapes associated with the moving point forces are almost identical between the two flow representations: see Figure 6.

The most readily apparent difference between the two is a shift in the location of the point force relative to the projectile boundary. Focusing of flow in the Landau-Squires jet means that as  $\mathcal{Re}_{NS}$  is increased the front stagnation point moves forward, away from the point force, while the enhanced inertia of the oncoming stream means that the stagnation point is pushed closer to the point force as  $\mathcal{Re}_O$  in the modified Oseen representation. The two representations also agree fairly well in respect of the component of the body-tangent component of the velocity field (Figure 7). The boundary of the scale-free shapes precisely demarcates the length scale on which the Navier-Stokes and modified-Oseen flow fields agree kinematically.

From the matching of two different singularity flows to two different far fields a sliver of fluid domain emerges in which velocities conveniently and surprisingly agree very closely between the two representations. Although the length scale of this domain can be easily computed, once it is known to exist, analytical explanation for what sets the length scale of this sliver, the final irreducible mystery of the modified Oseen's equations must be their ability to aligns features of the single-scale projectile shape over the entire of the separatrix.

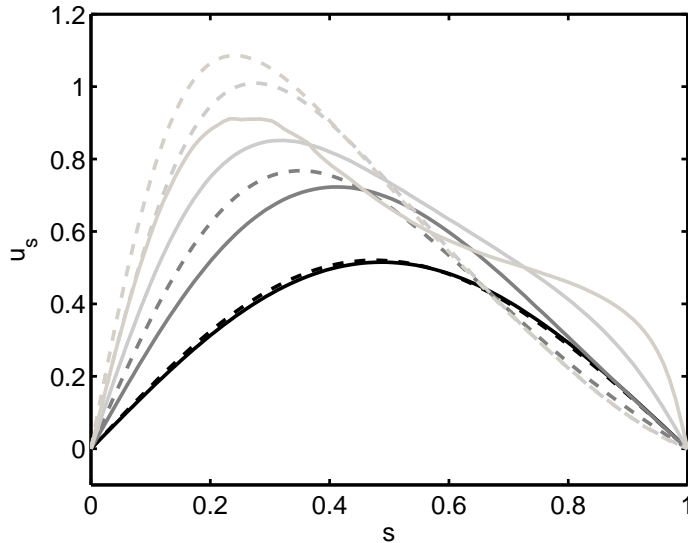


FIGURE 7. Comparison of tangential fluid velocities on the boundary of the single-scale shape between Navier-Stokes (solid curves) and modified-Oseen (dashed curves) representations of the flow. The location on the surface is denoted by scaled meridional arc length  $s$ , with the front stagnation point corresponding to  $s = 0$  and rear stagnation point to  $s = 1$ . The color key is shared with Figure 6.

## 6. Discussion

We have found a linear and reciprocal approximation to the Navier-Stokes equations that well-captures the drag-determining features of flows around steadily translating bodies. It was shown that the success of this approximation derives from its, incompletely understood, capacity to model the fluid drag on single-scale bodies. We note that the close concordance between approximate and exact representations for the drag can be violated by careful choice of sufficiently pathological projectile shapes and slip boundary conditions (Roper 2007).

We applied the approximation first to the classic problem of predicting the onset of separation in steady flow around a sphere, and of finding a functional form for the separated streamlines. Secondly, we devised a simple model for the growth or self-assembly of perfect projectiles, avoiding the need for complete knowledge of the flow field, in order to determine whether a particular test shape is optimal in respect of drag.

We are currently pursuing the natural and highly desirable generalisation of our linear approximation to unsteady flow effects. Neglect of such effects is acceptable for the modeling of micro-projectiles that are much denser than the fluid through which they travel, such as explosively launched fungal or plant propagules travelling through air (Vogel 2005). The flow around such bodies may be treated as quasi-steady, since the deceleration of the projectile will be much slower than the acceleration of the surrounding fluid mass. Unsteady effects assume primary importance only if the density contrast between body and fluid is not large. Nonetheless, an extension of the approximation to include unsteady effects would open up a large stable of additional problems. Many organisms live in or locomote through unsteady moderate- $Re$  fluid environments, and approximate models for the forces generated by the lift or thrust-generating limbs of flying insects (Wang 2005) or swimming planktonic organisms such as copepods (van Duren & Videler

2003) would enhance understanding of the physical challenges that these organisms have over-mastered.

This research is funded by the Kodak Fellowship and by the NSF Division of Mathematical Sciences. Discussions with Howard Stone and Todd Squires are gratefully acknowledged.

#### REFERENCES

- BATCHELOR, G. 1967 *Introduction to fluid dynamics*. C.U. Press.
- BRENNER, H. & COX, R. G. 1963 The resistance to a particle of arbitrary shape in translational motion at small Reynolds numbers. *J. Fluid Mech.* **17**, 561–595.
- CARRIER, G. 1953 On slow viscous flow. *Tech. Rep.* NR-062-163. ONR Mathematical Sciences Division.
- CHESTER, W. 1962 On Oseen’s approximation. *J. Fluid Mech.* **13**, 557–569.
- CHESTER, W. & BREACH, D. 1969 On the flow past a sphere at low Reynolds number. *Journal of Fluid Mechanics* **37**, 751–760.
- COX, R. 1965 The steady motion of a particle of arbitrary shape at small Reynolds numbers. *J. Fluid Mech.* **23**, 625–643.
- DAVIES, P. F. 1989 How do vascular endothelial cells respond to flow? *News. Physiol. Sci.* .
- DOMB, C. & SYKES, M. 1957 On the susceptibility of a ferromagnetic above the Curie point. *Proc. Roy. Soc. Lond. Ser. A* **240**, 214–228.
- VAN DUREN, L. & VIDELER, J. 2003 Escape from viscosity: the kinematics and hydrodynamics of copepod foraging and escape swimming. *J. Exp. Biol.* **206** (2), 269–279.
- VAN DYKE, M. 1970 Extension of Goldstein’s series for the Oseen drag of a sphere. *J. Fluid Mech.* **44**, 365–372.
- GOLDSTEIN, S. 1929a The forces on a solid body moving through a viscous fluid. *Proc. Roy. Soc. A* **123**, 216–225.
- GOLDSTEIN, S. 1929b The steady flow of viscous fluid past a fixed spherical obstacle at small Reynolds numbers. *Proc. Roy. Soc. A* **123**, 225–235.
- GOLDSTEIN, S. 1931 The forces on a solid body moving through a viscous fluid. *Proc. Roy. Soc. A* **131**, 198–208.
- INGOLD, C. 1971 *Fungal spores : their liberation and dispersal*. Oxford Clarendon Press.
- LABARBERA, M. 1990 Principles of design of fluid transport systems in zoology. *Science* **249**, 992–1000.
- LANDAU, L. & LIFSCHITZ, E. 1987 *Fluid Mechanics*, 2nd edn. Butterworth-Heinemann.
- MAXWORTHY, T. 1965 Accurate measurements of sphere drag at low Reynolds numbers. *Journal of Fluid Mechanics* **23**, 369–372.
- OSEEN, C. 1927 *Neuere Methoden und Ergebnisse in der Hydrodynamik*. Akademische Verlagsgesellschaft.
- PIRONNEAU, O. 1974 On optimum design in fluid mechanics. *J. Fluid Mech.* **64**, 97–110.
- PRINGLE, A., PATEK, S. N., FISCHER, M., STOLZE, J. & MONEY, N. P. 2005 The captured launch of a ballistospore. *Mycologia* **97**, 866–871.
- PROUDMAN, I. & PEARSON, J. R. A. 1957 Expansions at small Reynolds numbers for the flow past a sphere and a circular cylinder. *J. Fluid Mech.* **2**, 237–262.
- READ, N. & BECKETT, A. 1996 Ascus and ascospore morphogenesis. *Mycol. Res.* **100**, 1281–1314.
- ROPER, M. 2007 Symmetry breaking and un-breaking in micro-hydrodynamical systems: locomotion, sheared suspensions and bio-ballistics. PhD thesis, Harvard School of Engineering and Applied Sciences.
- ROPER, M., SQUIRES, T. & BRENNER, M. 2007 Unbroken symmetry of perfect projectiles. Submitted to *Phys. Fluids*.
- SHRAIMAN, B. 2005 Mechanical feedback as a possible regulator of tissue growth. *Proc. Nat. Acad. Sci.* **102**, 3318–3323.
- TANEDA, S. 1956 Experimental investigation of the wake behind a sphere at low Reynolds numbers. *J. Phys. Soc. Jpn.* **11**, 1104–1108.

- VEYSEY, J. & GOLDENFELD, N. 2006 Singular perturbations in simple low Reynolds number flows: from boundary layers to the renormalization group. *Arxiv preprint physics/0609138*
- VOGEL, S. 2005 Living in a physical world II. The bio-ballistics of small projectiles. *J. Biosci.* **30**, 167–175.
- WANG, Z. J. 2005 Dissecting insect flight. *Ann. Rev. Fluid Mech.* **37**, 183–210.